Effects of resonant magnetic perturbations on turbulence and flows in the edge of HL-2A plasmas

Cite as: Phys. Plasmas **31**, 042502 (2024); doi: 10.1063/5.0191468
Submitted: 14 December 2023 · Accepted: 12 March 2024 ·
Published Online: 1 April 2024

Jingchun Li,[1,2] Z. Lin,[3] J. Cheng,[4] Z. X. Wu,[1,a)] Jianqiang Xu,[5] Y. He,[5] Z. H. Huang,[5] A. S. Liang,[5] T. F. Sun,[5] J. Q. Dong,[5] Z. B. Shi,[5] Wulyv Zhong,[5,a)] M. Xu,[5] and HL-2A Team[5]

AFFILIATIONS

[1]Shenzhen Key Laboratory of Nuclear and Radiation Safety, Institute for Advanced Study in Nuclear Energy & Safety, College of Physics and Optoelectronic Engineering, Shenzhen University, Shenzhen 510640, People's Republic of China
[2]Department of Earth and Space Sciences, Southern University of Science and Technology, Shenzhen, Guangdong 518055, People's Republic of China
[3]University of California, Irvine, California 92697, USA
[4]Institute of Fusion Science, School of Physical Science and Technology, Southwest Jiaotong University, Chengdu 610031, People's Republic of China
[5]Southwestern Institute of Physics, P.O. Box 432, Chengdu 610041, People's Republic of China

[a)]**Authors to whom correspondence should be addressed:** zhongwl@swip.ac.cn and wuzhx@szu.edu.cn

ABSTRACT

The influence of resonant magnetic perturbations (RMPs) on the dynamics of turbulence and flows at the edge of the HL-2A tokamak is analyzed utilizing transfer entropy technique. The results have shown that the RMP damps the poloidal flows as well as the $\mathbf{E} \times \mathbf{B}$ shearing rate, whereas enhances the toroidal flows and leads to a broadened particle spectrum with increased small scale turbulence transport. The causality analysis indicates that the regulation impact of poloidal flow on turbulent fluctuations and particle flux is weakened, while that of the toroidal rotation on the latter is strengthened by the RMP field. The impact of the changes in poloidal flow dominates over that of the modified toroidal flow on turbulent transport in the edge. The magnetic perturbation and the flows generally show predator–prey oscillations, where the causal effect between the former and the toroidal flow transits to a synchronization relation in the presence of RMP. In addition, the RMP field will weaken the causal effect on poloidal Reynolds stress while strengthening the parallel-radial component simultaneously. The present findings provide a possible explanation on the effects of external fields on the edge transport, which is suggested to be dominated by the complex interactions among external perturbations, flows, and ambient microturbulence.

I. INTRODUCTION

The perturbing magnetic fields generated by the resonant magnetic perturbation (RMP) coils[1] were used for modifying the edge transport, magnetohydrodynamic (MHD) stability, and turbulence properties with many machines operating a variety of in- and ex-vessel saddle coils over the last several decades since the early application of RMPs on TEXT and JFT-2M in the 1990s.[2–4] Plenty of experiments on many tokamaks have demonstrated that the small RMP fields due to external coils can lead to a variety of unexpected effect on the plasmas, which will affect the overall confinement and stability of the plasma substantially, including the altering of tearing modes (TMs),[5,6] small-scale turbulence,[7–12] low to high confinement mode (L-H) transition thresholds,[7,13,14] and so on. One of the most important progresses in using RMPs lies in the aspect of controlling large type-I edge localized modes (ELMs)[15–17] during H-mode, and the physical understanding of plasma response as well as the characteristics of edge fluctuations in the presence of RMP fields still remains an open issue, which is particularly important for next step fusion devices such as ITER.[18]

The RMPs are large-scale magnetic fluctuations imposed on plasma equilibria through the utilization of currents driven in external coils. The local turbulence and flows are influenced in several ways, for example, the formation of stochastic layers or ergodic zones in the edge region induced by the change of the magnetic topology. During the ergodic divertor (ED) operation on TEXT[3] and Tore Supra,[19] an intriguing phenomenon has been witnessed where the presence of

large-scale turbulent cells is effectively suppressed, leading to a remarkable reduction in density fluctuations. It has been observed in the dynamic ergodic divertor (DED) experiments on the TEXTOR tokamak that the potential fluctuations exhibit a significant reduction, accompanied by a remarkable change in the direction of local turbulent flux with the suppression of large-scale structures and a decrease in both radial and poloidal correlation lengths.[20,21] Despite those benefits in demonstrating sustained confinement in tokamaks, the intricate nonlinear response of the plasma to RMPs remains a complex phenomenon that has yet to be fully comprehended. In addition to the direct increase in H-mode pedestal transport and stability to prevent peeling–ballooning modes[22] serving as the driver for ELMs, the situation is more complicated in L-modes as in the latter case the edge region generally shows the existence of meso-scale zonal flows (ZFs),[23] especially the high branch geodesic acoustic modes (GAMs),[24] which are usually weak in H-mode scenarios. For example, on MAST spherical tokamak, the impact of the RMPs on the density fluctuations and the evolution of the poloidal and toroidal flows in L-mode plasmas have been reported, where the poloidal and toroidal flows tend to decrease and increase inside the separatrix, respectively.[25] Any coupling to magnetic field perturbations opens an additional transport channel, thus could provide a significant mechanism for turbulent transport. Hence, a comprehensive exploration of the properties of the nonlinear interactions among these magnetic perturbations, flow fluctuations, and background microturbulence represents a crucial endeavor in elucidating the fundamental mechanisms governing fusion plasmas.

Although theories and experiments mainly focus on the impact of RMPs on edge pedestal stability and ELM control, it is generally more convenient to operate in regimes where the edge turbulence behavior is easy to be detected and analyzed in order to investigate the fundamental physics of interactions among turbulence, flows, and RMPs, namely, the low density Ohmic or L-mode edge plasmas.

More importantly, in addition to the conventional analysis such as cross-correlation or spectrum methods, which measure the similarity between two signals in the time or frequency domain, our current understanding of the "*causal*" impact of RMPs on turbulence remains limited due to the absence of a suitable causality analysis method. Traditional correlation analysis can yield misleading or inaccurate conclusions regarding causality, as highlighted by the well-known adage "*correlation does not imply causation.*"[26] Therefore, it is imperative to employ a precise mathematical causality approach to carefully investigate the causal influence of RMPs on edge flows and turbulence, which constitutes the primary objective of this study.

The paper is organized as follows: In Sec. II, we provide a detailed description of the experimental setup and the techniques employed for causality analysis. In Sec. III, we present the experimental analysis results obtained from the RMP modulation experiments conducted in the edge plasmas of HL-2A. Finally, conclusions and discussions are drawn in Sec. IV.

II. EXPERIMENTAL SETUP AND TRANSFER ENTROPY (TE) TECHNIQUE

A. Experimental setup

The RMP modulation experiments were performed in ohmically heated deuterium plasmas in the HL-2A tokamak[27] (major radius $R = 1.65$ m and minor radius $a = 0.4$ m) with typical parameters of

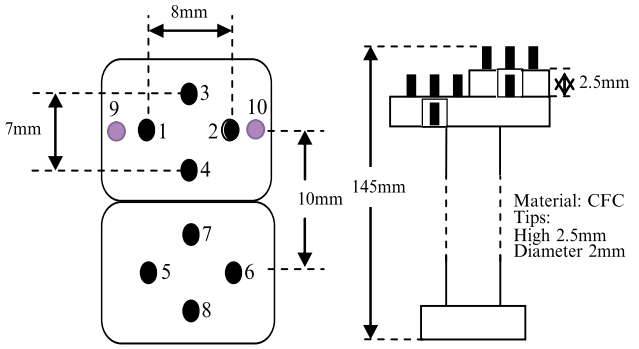

FIG. 1. Sketch of the fast reciprocating probe array on HL-2A.

plasma current $I_p \approx 130$ kA, toroidal magnetic field $B_T \approx 1.37$ T, and core line-averaged density $\bar{n}_e \approx 0.9$–1.0×10^{19} m^{-3} during the steady state. The $n = 1$ RMP fields were applied with coil current $I_{coil} = 5$ kA and duration time of 50 ms. The plasma edge fluctuations were measured in the boundary region using a high-speed reciprocating Langmuir probe (LP) system positioned at the outer middle plane. This LP system, as depicted in Fig. 1, has previously been employed in studies on sheared flow dynamics[28] and L-H transitions.[29] The LP data were acquired with a sampling frequency of $f_s = 1$ MHz and 12-bit precision, with negligible perturbation of the plasma induced by the probe array. Local physical quantities were computed utilizing the triple-tip principle.[30] For instance, the pins numbered by (1, 2) and (5, 6) are pairs of standard double probes used to sample the ion saturation current, $I_{s1(2)} = (V_{1(5)} - V_{2(6)})/R_s$ with R_s being the sampling resistance. Pin pairs numbered by (3, 4) and (7, 8) are used for detecting floating potentials (ϕ_f), from which the radial and poloidal electric fields E_r and E_θ can been deduced from the two radially and poloidally separated pins as $E_r = (\phi_{f4} - \phi_{f7})/\Delta r$ and $E_\theta = (\phi_{f3} - \phi_{f4})/\Delta\theta$, where the distances are $\Delta r = 2.5$ and $\Delta\theta = 7.0$ mm, respectively. The local electron temperature and density are, thus, calculated as $T_{e1} = [V_2 - (\phi_{f3} + \phi_{f4})/2]/\ln 2$ and $n_{e1} = 2I_{s1}/[eA_{eff}(k_b T_e/m_i)^{0.5}]$, where A_{eff}, k_b, and m_i stand for the effective collecting area of 10.0 mm^2, the Boltzmann constant, and the ion mass, respectively. The Mach probe[31] array is utilized to measure the local plasma rotation, and the toroidal flow velocity denoted by the Mach number is evaluated as $M_{||} \approx 0.4\ln(I_{s9}/I_{s10})$, where the sheath currents, denoted as I_{s9} and I_{s10}, are measured on two Mach probe tips located at the up- and downstream sides, respectively. By estimating the Mach number and measuring the electron temperature, the toroidal velocity can be determined as $V_{||} \approx M_{||}c_s$, where the ion sound speed is calculated as $c_s = \sqrt{2T_e/m_i}$.

B. Transfer entropy technique

In this paper, the analysis methods used to characterize the causal influence of RMP on edge turbulence and flows are mainly two-point and transfer entropy (TE) techniques.[32] Here, we only give a brief description of the latter. Transfer entropy, a concept originating from Information Theory, provides a distinct approach to assess causal relationships between time series. Unlike traditional correlation measures, transfer entropy is directional and enables the detection of information flow between correlated sequences. This nonlinear technique quantifies the "*information transfer*" between two signals, incorporating all

available information irrespective of amplitude or sign. It was recently applied in fusion plasmas in order to quantify the *causal* impact of zonal flows on turbulent[33] and multi-scale interactions among tearing modes, zonal flows, and turbulence,[34] which have indicated that it is a powerful tool for the analysis of causal relations in complex systems.

By simultaneously examining the measured signals X and Y, which result in discretely sampled time series data x_i and y_j, the transfer entropy quantifies the enhancement in predicting the next sample of signal X through the utilization of not only its own time history but also that of signal Y. In a simplified manner, the transfer entropy can be expressed using the following formula:

$$TE_{Y\to X}(k) = \sum p(x_{N+1}, x_{N-k}, y_{N-k}) \log_2 \frac{p(x_{N+1}|x_{N-k}, y_{N-k})}{p(x_{N+1}|x_{N-k})}. \quad (1)$$

To construct the probability distributions $p(a, b, c, \ldots)$ in our analysis, we divide each argument into m bins, resulting in a total of m^d bins for the object $p(a, b, c, \ldots)$. Here, d represents the dimension of p. The probability distribution $p(x|y) = p(x, y)/p(y)$ represents the conditional probability distribution of x conditional on y. The length of the signal is denoted as N, and the time-delay embedding vector k can be converted to a "time lag" by multiplying it with the sampling time, denoted as $\Delta\tau = k/f_s$.[35] The sum in equation runs over the corresponding discrete bins. Low number of bins (here $m = 2$ or 3), termed as "*course graining*," are used in the construction of the probability distributions in order to obtain statistically significant results. Transfer entropy quantifies the information transfer or the reduction of uncertainty in predicting one variable using another variable. It measures the increased accuracy in signal prediction based on available observations. Further details on this technique can be found in Ref. 33. The transfer entropy, measured in bits, can be compared to the maximum possible value of $\log_2 m$, representing the total bit range, to assess the significance of the information transfer. By calculating the TE with varying time delays, the temporal scale of the maximum impact of one variable on another can be accurately captured. In modulation systems, there is typically a time delay between the influence of one physical quantity on another. The TE allows the identification of the true time delay when the strongest information flow and causal impact of magnetic fluctuations or flows on turbulence are at their maximum. Notably, previous studies[34] have demonstrated that the TE not only reflects maximum coherence but also the highest causal effect, as evidenced by the nearly simultaneous occurrence of maximum cross correlation and TE values at the same time lag.

III. EXPERIMENTAL RESULTS

In this section, the experimental results of the causal relations among magnetic fluctuations induced by RMPs, flows, and edge turbulence are presented based on the transfer entropy analysis technique. Figure 2 shows the typical discharge waveforms of the RMP modulation experiments and the local physical quantities measured by the probes. The edge equilibrium electron density and temperature measured by LPs are also kept almost constant, while their fluctuations are strongly influenced by the external RMP fields (not shown here). The plasma shape and flux surfaces calculated by the kinetic equilibrium and reconstruction fitting module (kinetic EFIT) incorporated in the framework of OMFIT integrated modeling[36] together with the profiles of safety factor q as well as the magnetic shear $\hat{s}$ regarding the phases with and without RMPs are illustrated in Figs. 2(b) and 2(c). It is

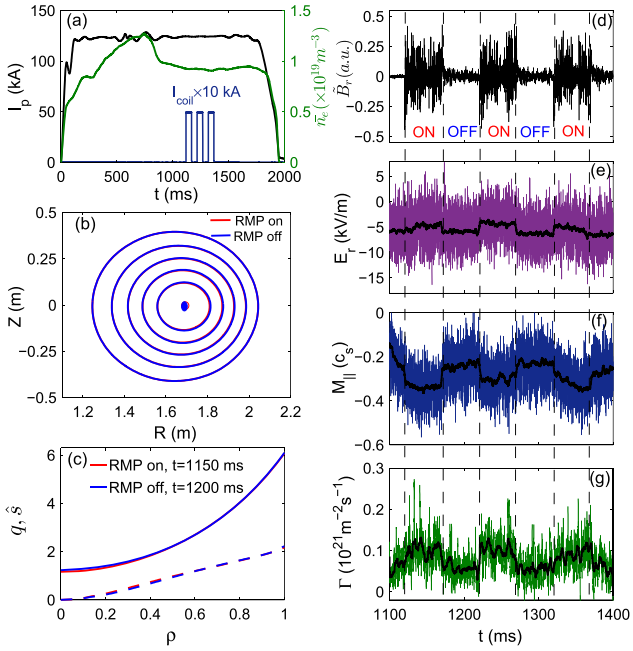

FIG. 2. Left panel: (a) discharge waveforms of plasma current I_p, central line-averaged density $\bar{n}_e$, and RMP coils current I_{coil}, (b) plasma surface shapes, (c) safety factor q and magnetic shear $\hat{s}$ profiles. Right panel: time evolutions of (d) radial magnetic fluctuation $\tilde{B}_r$, (e) radial electric field E_r, (f) Mach number $M_{||}$, and (g) particle flux Γ during the RMP modulation experiments.

clearly indicated that plasma equilibrium exhibits a circular geometry in both phases, and it is noted that the q profile only slightly differs in the core region, whereas they are almost identical at the edge when RMP is turned on. A significant increase in the radial magnetic fluctuation ($\tilde{B}_r$) is detected on the radial Mirnov coils during the RMP period, which can be seen in Fig. 2(d). It is noted that although the precise value of $\tilde{B}_r$ cannot be given due to the lack of calibration, it does not affect the values of transfer entropy because TE is independent of the amplitudes of the signals. The probes are inserted into the plasma whose position with respect to the last closed flux surface (LCFS) is around $r - r_{\mathrm{LCFS}} \approx -2.5$ cm, corresponding to the normalized position of $\rho \approx r/a = 0.93$. The radial electric field E_r and Mach number $M_{||}$ deduced from LP data are shown in Figs. 2(e) and 2(f), respectively, from which a clear decrease in E_r amplitude is observed, whereas an increase in $M_{||}$ is found as long as the RMP is turned on. The local particle flux formulated as $\Gamma_r = \langle \tilde{n}_e \tilde{E}_\theta \rangle / B_T$ is shown by Fig. 2(g), where $\langle \cdot \rangle$ denotes the ensemble average.[37] The enhancement of edge transport might be explained by two reasons: one is that the stochastization of the edge magnetic field lines would lead to a larger cross field transport directly. The other is that the changes in local E_r and its shear can change transport locally and the zonal flow damping is enhanced in the presence of RMP fields;[38] hence, the transport is increased, although only relatively weak geodesic acoustic modes are present in the edge region of these experiments.

Based on the above-mentioned measurements, the causal relations among magnetic fluctuations, flows, and turbulence are calculated. In order to give a basic understanding of the causal relations, it is the most convenient way to estimate the spectra of the background

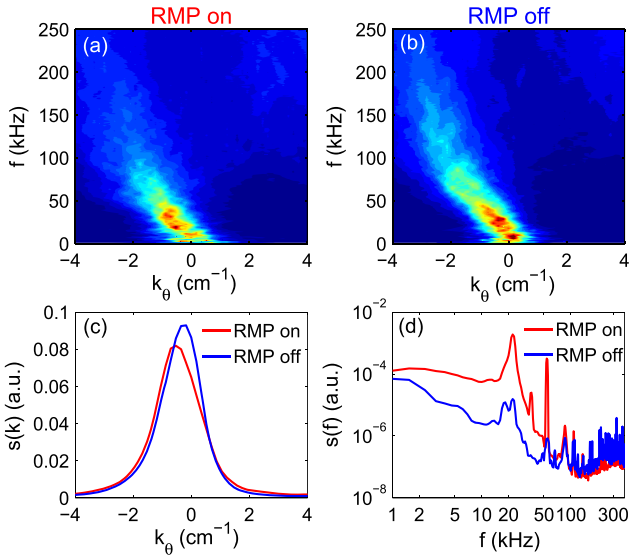

FIG. 3. Local statistical wavenumber-frequency spectra of the background turbulence (a) with and (b) without RMP. Comparison between (c) wavenumber spectra and (d) power spectra of density fluctuations with (red) and without (blue) RMP.

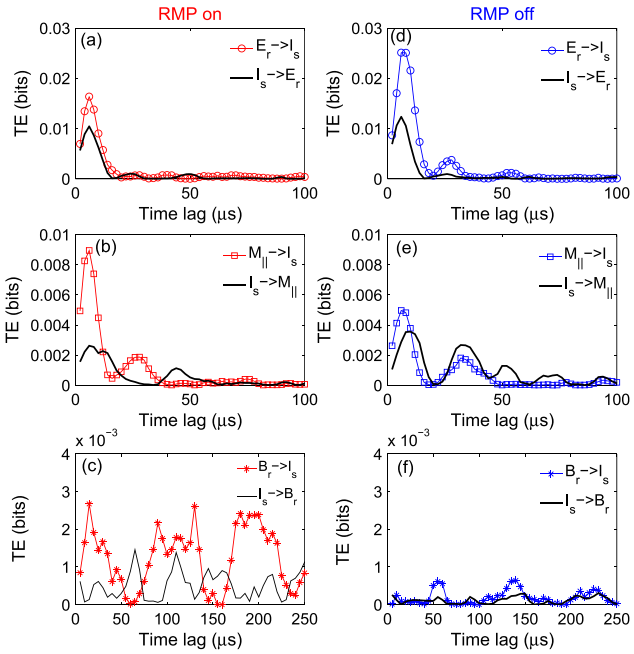

FIG. 4. Transfer entropy as a function of time lag between poloidal flow, toroidal flow, and radial magnetic field and density fluctuations. (a)–(c) The causal relations with RMP fields, while (d)–(f) are that without RMP, respectively.

turbulence at first so as to demonstrate the changes of the turbulence behavior due to external fields. The local wavenumber-frequency spectra $S(k, f)$ with and without RMP computed by the two-point method[39] using data from two poloidal separated pins are shown in Figs. 3(a) and 3(b), respectively. The spectrum $S(k,f)$ is defined as $S(k,f) = \frac{1}{M}\sum_{j=1}^{M} I_{\Delta k}[k - k^j(f)]\left|S_1^j(f) + S_2^j(f)\right|/2$, where $I_h(x)$ is the indicator function. The power spectra, denoted as S_1^j and S_2^j, are obtained from measurements at two distinct positions with a separation of $\Delta x \leq \pi/k_{max}$. The maximum wavenumber of the fluctuations to be measured is denoted as $k_{\max}$. The local wavenumber is represented by $k^j(f) = \Delta\theta_{12}^j(f)/\Delta x$, and $\Delta\theta_{12}^j(f)$ represents the phase shift between the two points for each realization j. The total number of realizations is denoted as M. The background turbulences show the drift-wave type dispersion relation in both cases where the poloidal wavenumber spectrum is more peak when RMP coil current is turned off, as shown in Fig. 3(c). In addition, the peak wavenumber shifts to the short wavelength side in the presence of the external RMP fields. The spectrum of background density fluctuations illustrated in Fig. 3(d) indicates that the RMP fields mainly act on the low frequency turbulence, typically in the range of $f < 50$ kHz especially the turbulence peaks around $f \sim 20$ kHz, whereas the high frequency fluctuations are almost unaffected by the RMPs. These results from the spectral analysis suggest that the RMPs have strong impact on the low frequency fluctuations or large scale turbulence.

The causal impact of poloidal and toroidal flows (donated by E_r and $M_{||}$) as well as the radial magnetic field B_r on density fluctuations is depicted in Fig. 4. Here, the ion saturation current fluctuation $\tilde{I}_s$ is used, which is approximately proportional to the density fluctuations $\tilde{n}_e$, and it has already proven that this approximation is valid in probe analysis especially for the low temperature plasmas such as in the edge of fusion devices.[40] The values of information transfer donated by TE as a function of time lag k in sampling units μs are obtained using a typical data length of 20 ms. The first peak values between $\tilde{E}_r$ and $\tilde{I}_s$ are relatively large for both cases, i.e., $TE \sim 2.0 \times 10^{-2}$, indicating that the causal link between the two physical quantities is strong. Meanwhile, it is observed that the value of $TE_{\tilde{E}_r \to \tilde{I}_s}$ without RMP fields is larger, which demonstrates that the poloidal flow has a more significant impact on the background fluctuation, as can be concluded by the comparison between Figs. 4(a) and 4(d). On the contrary, the causal relations between toroidal flows and density fluctuations shown in Figs. 4(b) and 4(e) suggest that the influence of toroidal flows on turbulence is enhanced when RMP is applied. It is also noted that the impact of poloidal flows on turbulence is more significant than the toroidal rotation. Furthermore, an oscillation feature is found, which is more obvious without RMPs, implying that the modulation effects of flows on turbulence and the backward reactions are stronger. The physics might be strongly related to the direct increase in the causal impact of external magnetic fields on turbulence, as can be found in Figs. 4(c) and 4(f). The modulation periods of B_r on $\tilde{I}_s$ are around 50–70 μs in both situations, which is consistent with the observation of a mode with central frequency around $f \sim 20$ kHz whose fluctuation amplitude becomes higher in the presence with RMPs as compared to without RMPs. The results underline the important and strong nonlinear coupling between external fields and turbulence within a certain frequency range. The underlying mechanisms cannot be identified yet and should be objects of further research, which are beyond the goal of the present study. The analyses have also implied that the coupling between turbulence and poloidal flow is weakened due to RMP field, leading to an increased transport at the edge plasmas.

Figure 5 illustrates the causal impact of magnetic fluctuations on flows. It is discovered that the external B_r has strong impact on the information flow in terms of transfer entropy. The quasi-oscillation

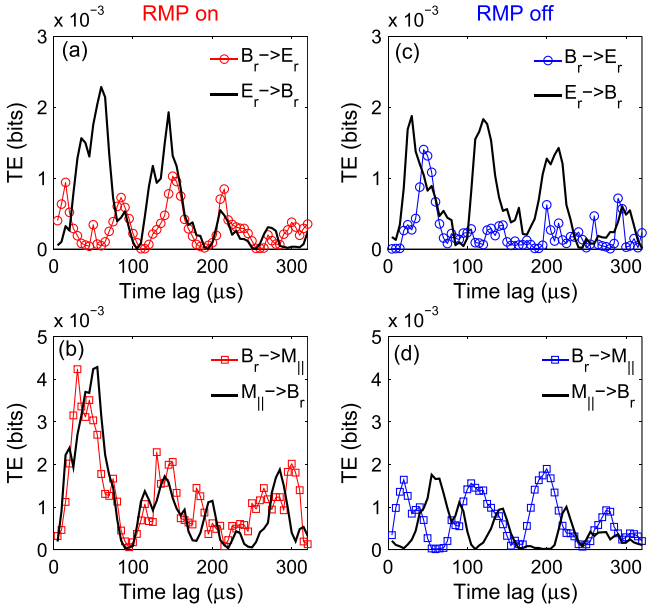

FIG. 5. Causal relations between magnetic perturbations and flow fluctuations. (a) and (b) The causal impact of B_r on E_r and $M_{||}$ during RMP, while (c) and (d) are that without RMP, respectively.

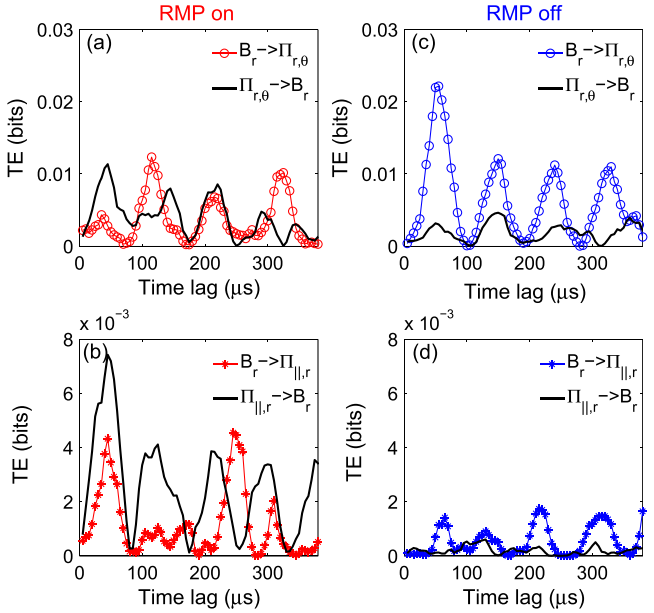

FIG. 6. Transfer entropy as a function of time lag between magnetic perturbations and Reynold stresses. (a) and (b) The causal impact of B_r on $\Pi_{r,\theta}$ and $\Pi_{||,\theta}$ during RMP, while (c) and (d) are that without RMP, respectively.

features appearing in the relations have suggested that the magnetic fluctuations and flow perturbations would form a modulation system. The presence of RMP fields can modify the modulation effects of B_r on poloidal flows, i.e., B_r modulates E_r within a shorter timescale and the latter acts back on a longer one when RMP is present. On the contrary, the maximum causal impact of B_r on poloidal flow lags behind in the backward reaction in the absence of external fields, as can be concluded by the comparison between Figs. 5(a) and 5(c). The interaction between B_r and $M_{||}$ shows a synchronization feature during RMP, which can be clearly seen in Fig. 5(b). However, when the causal impact of B_r on toroidal flow is maximum, the backward process reaches minimum in the absence of RMPs, and vice versa, which can be seen in Fig. 5(d). The above-mentioned relations have suggested that the causal impact of B_r on flows may depend on the magnitude of radial magnetic fluctuations, which would show a predator–prey oscillation with an inphase and antiphase relation for large and small amplitudes of externally imposed magnetic perturbations, respectively.

The previous findings using causality analysis method in terms of transfer entropy have clearly indicated that the external magnetic field perturbations generated by RMP coils have direct causal impact on turbulence and flows; thus, it is no doubt that these fields will affect the Reynolds stress (RS), including both poloidal- and parallel-radial terms, which are suggested to be responsible for the zonal flow generation[41] and momentum transport/redistribution as well as the intrinsic rotation,[42] respectively. The role of Maxwell stress is not important in the edge plasma of Ohmic discharges but needs further study in the future. Figure 6 shows the causal relations between RMP component and the stresses, where the poloidal and parallel radial stresses are defined $\Pi_{r,\theta} = \langle \tilde{v}_r \tilde{v}_\theta \rangle = -\langle \tilde{E}_r \tilde{E}_\theta \rangle / B_T^2$ and $\Pi_{||,r} = \langle \tilde{v}_{||} \tilde{v}_r \rangle = -\langle \tilde{M}_{||} \tilde{E}_\theta \rangle \frac{c_s}{B_T}$, respectively. It is interesting that the RMP can change the causility significantly. In the absence of RMP, B_r and $\Pi_{r,\theta}$ show a synchronization relationship and the modulation effect of the former on the latter is stronger than the inverse process, while the causal effect of B_r on $\Pi_{||,r}$ is very weak although a regulation feature can be discovered, as shown in Figs. 6(c) and 6(d), respectively. On the contrary, B_r has strong modulation and causal effect on $\Pi_{r,\theta}$ in the presence of RMP, which can be seen in Fig. 6(b). As the enhancement in the radial magnetic fluctuations is mainly caused by the RMP fields [see Fig. 2(d)], it is strongly suggested that RMP could modify the momentum distribution in the edge plasma due to its three dimensional nature. Meanwhile, the RMP also modifies the causal effect of B_r on $\Pi_{r,\theta}$, where it shows that causal and modulation influence on $\Pi_{r,\theta}$ decreases, whereas the inverse process is increased, respectively, as can be inferred from Figs. 6(a) and 6(c). These findings imply that the external magnetic fluctuation induced by RMPs may reduce or enhance the amplitudes of zonal flows and intrinsic rotation. Although previous experimental and simulations have indicated that the RMP can damp the ZFs, such as GAMs in the edge region,[25,43] it is not clear how the former acts on the latter. Our results suggest that the weakened ZFs and intrinsic rotations resulted from the enhanced causality between magnetic and electrostatic fluctuations, where information flow from Reynolds stresses to the magnetic perturbations becomes larger in the presence of RMP; thus, the coupling between stresses and other electrostatic modes, such as GAMs, decreases, leading to a weaker ZF amplitude as long as RMP is applied.

The effect of RMPs on the causal relations between E_r and transport flux Γ_r is shown in Fig. 7. It should be noted that the time lags when the TEs are maximum do not represent the decorrelation time deduced from cross correlation function of turbulent fluctuation as they have rather different meanings, i.e., the former is the time when the information flow from a cause to an effect reaches greatest, where the latter donates the maximum linear similarity when a time sequence

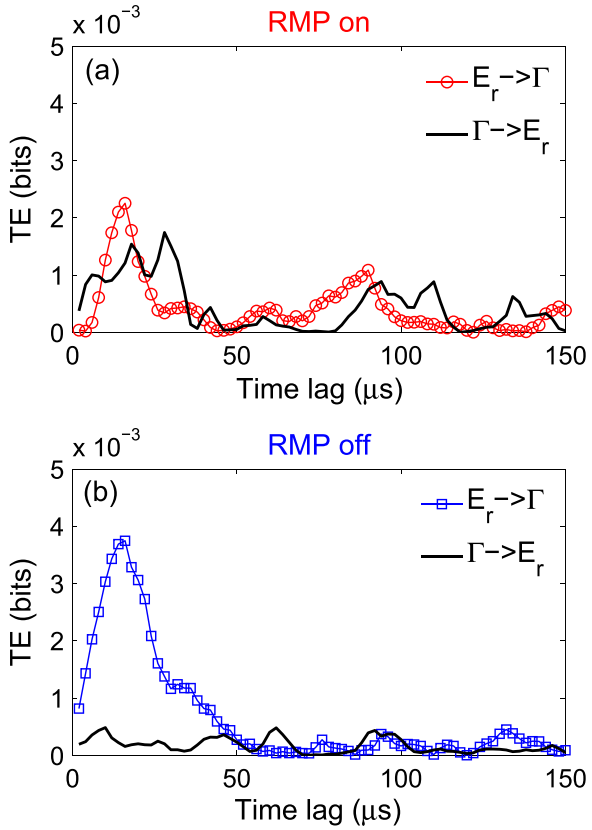

FIG. 7. Causal relations between radial electric field E_r and particle flux Γ_r. (a) with RMP and (b) without RMP.

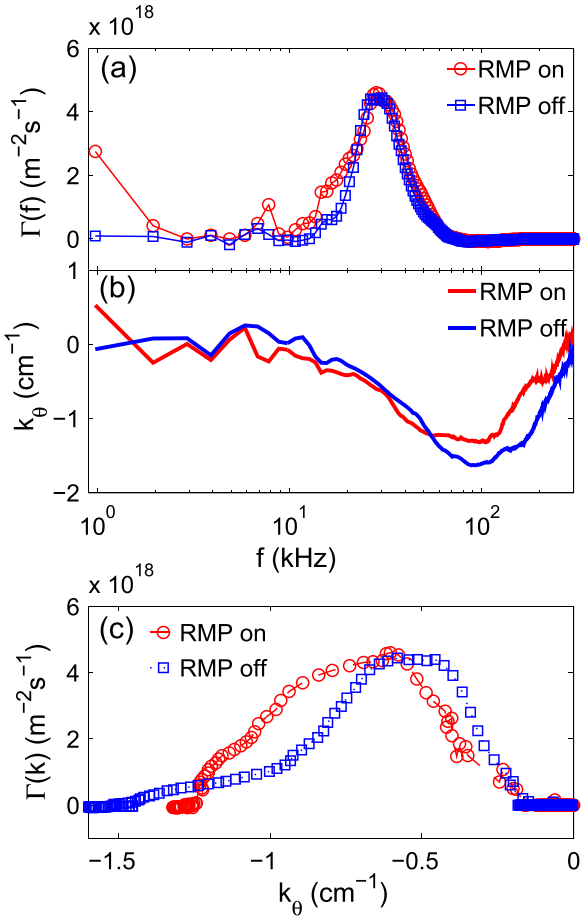

FIG. 8. Frequency spectra of (a) particle flux and (b) mean poloidal wavenumber. (c) The corresponding wavenumber spectrum of flux. The results with and without RMP are donated by red and blue curves, respectively.

is lagged. It can be found that the causal influence of E_r on transport is decreased due to RMP during the timescale less than 50 μs, leading to an enhancement of edge transport during the RMP, as previously demonstrated in Fig. 2(g).

The comparison of flux spectra with and without RMP is shown in Fig. 8. The mean poloidal wavenumber is estimated as $k(f) = \sum_k k \cdot S(k|f)$, and flux spectrum is calculated by $\Gamma(f) = \frac{2}{B_T} k(f) |P_{\tilde{n}\tilde{\phi}}(f)| [\sin \alpha_{\tilde{n}\tilde{\phi}}]$, where $P_{\tilde{n}\tilde{\phi}}$ and $\alpha_{\tilde{n}\tilde{\phi}}$ denote the cross power and phase shift between density and floating potentials, respectively. It is noted that the RMP field modifies the transport induced by low frequency fluctuations with $f < 30$ kHz, especially those with $f < 5$ kHz as shown in Fig. 8(a). However, the wavenumber spectrum is mainly modified in the high frequency range as can be found in Fig. 8(b). As a result, the combined effects lead to a broadened wavenumber spectrum of flux with RMPs applied, particularly on the large wavenumber side, indicating that the RMP would cause lots of small scale turbulence structures as well as the increased transport level, as can be seen in Fig. 8(c). Such results might be explained by the chaotization of the field lines in the edge region in the presence of a RMP field; thus, the turbulent vortex structures, which have initially regular shapes, are disorganized and teared apart according to the rearrangement of edge magnetic topology.

The effect of RMP on the perpendicular velocity donating the radial electric field is plotted in Fig. 9(a). The data were obtained by the Doppler reflectometry[44] and averaged over 20 ms for each phase. A slight decrease in the velocity over the whole measured region of $\rho > 0.5$ is observed when RMP is turned on. However, the corresponding shearing rate, $\omega_{E\times B} = \frac{2\pi d v_\perp}{B_T dr} \approx \frac{2\pi R_0 d v_\perp}{a B_T d\rho}$, is almost unaffected inside $\rho < 0.8$. The $\mathbf{E} \times \mathbf{B}$ shearing rate is decreased mainly in the edge region of $0.85 < \rho < 0.95$ corresponding to the zero-crossing of the velocity, as the RMPs fields damp the rotation, making both the positive and negative velocities more closer to zero simultaneously. As a result, the main changes in shearing rates locate around the zero velocities, as indicated in Fig. 9(b). The auto-correlation functions (ACFs) of the floating potentials during each phase are illustrated by the insert, from which it is estimated that the turbulence decorrelation times defined as the e-folding time of the ACFs, are around $\tau_d \approx 10$ and 6 μs whose inverse is comparable to the shearing rates $\omega_{E\times B} \sim 1.3 \times 10^5$ and 1.8×10^5 Hz for the case of with and without RMP, respectively. The results have confirmed that although the RMP will modify both the turbulence and radial electric field, the general perception of turbulence decorrelation by $\mathbf{E} \times \mathbf{B}$ shear is still satisfied, especially in the plasma edge where the toroidal rotational shear is weak and the shearing rate is primarily determined by poloidal rotation.

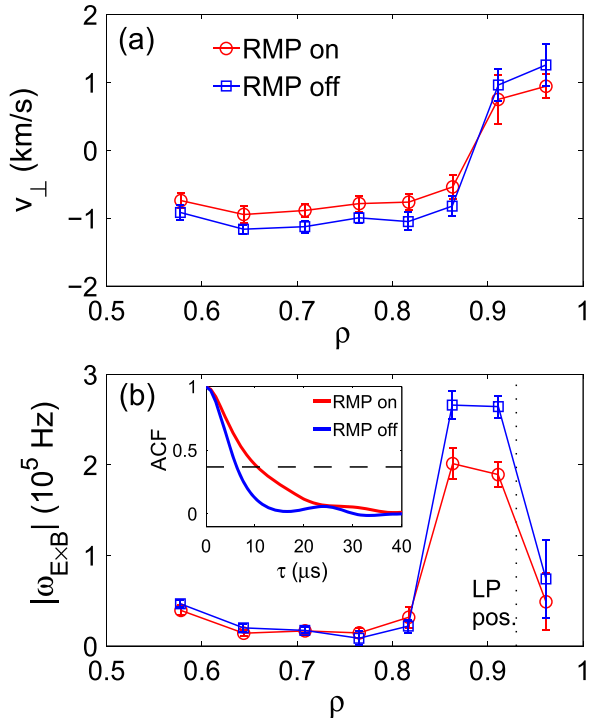

FIG. 9. Radial profiles of (a) perpendicular velocity and (b) $\mathbf{E} \times \mathbf{B}$ shearing rate. The auto-correlation function calculated from floating potentials is plotted by the inset, and the vertical dashed line donates the LP position. The results with and without RMP are shown by red and blue curves, respectively.

Although the above-mentioned findings have clearly shown that the edge turbulent transport is enhanced due to the external fields, it is difficult to determine which physical parameter is critical for the transport at present. According to recent theories and simulations, a key parameter that controls the edge transport of Ohmic or L-mode plasmas is the $\mathbf{E} \times \mathbf{B}$ shearing rate. However, it should be pointed out that although it has clearly shown that change in the edge turbulent transport is due to the variation of the normalized $\mathbf{E} \times \mathbf{B}$ shearing caused by RMP, a clear understanding of the RMP fields on turbulence and flows are still missing at the moment. The three dimensional nature of the external fields and the nonlinear interactions between magnetic topology and turbulence might play the key role, which will be left for future works.

IV. CONCLUSIONS

In this work, the effect of RMP on edge flows and transport is analyzed utilizing transfer entropy technique. It is shown that the edge poloidal flow is damped, while the toroidal flow is increased due to the external fields. The turbulence spectrum is broadened, and the small scale turbulent transport is enhanced by the RMP. The $\mathbf{E} \times \mathbf{B}$ shearing rate is decreased mainly in the edge region as the penetration depth of the RMP fields is limited. However, it has been confirmed that the $\mathbf{E} \times \mathbf{B}$ shearing decorrelation mechanism is still satisfied especially in the plasma edge where the shearing rate is predominated by the poloidal flow although the RMP will modify both the turbulence and radial electric field. Causality analysis results have shown that the modulation effect of poloidal flow on turbulence and particle flux is weakened, whereas the toroidal flow on density fluctuations is enhanced when RMP is applied, during which the former is more significant than the latter. The magnetic fluctuation induced by RMP and the toroidal flow show a predator–prey oscillation depending on the amplitudes of externally imposed magnetic perturbations. Moreover, the RMP field modifies the causal and modulation effects between magnetic fluctuation and Reynolds stresses, showing that the magnetic fluctuation induced by the RMP weakens these effects on poloidal term, while the effect on parallel-radial term is strengthened, implying that the weakened ZFs and intrinsic rotations are resulted from the enhanced causality between magnetic and electrostatic fluctuations due to the decreased coupling between stresses and coherent modes such as GAMs. Thus, it is claimed that the enhancement of edge transport during RMP might be resulted from the combined effects of the reduction of zonal flow drive and mean poloidal flow shearing. However, the detailed nonlinear simulations involving three dimensional effects are certainly necessary in future works.

ACKNOWLEDGMENTS

This work was partly supported by National Key R&D Program of China (Grant Nos. 2019YFE03020004 and 2022YFE03060002), National Natural Science Foundation of China (Grant Nos. 12275071, 12261131622, and 12125502), China National Nuclear Corporation Fundamental Research Program (Grant No. CNNC-JCYJ-202236), Sichuan Science and Technology Program (Grant Nos. 2021JDJQ0029 and 2023NSFSC1289), the Italian Ministry of Foreign Affairs (Grant No. CN23GR02), Fourteenth Five-Year Plan Basic Technological Research Project (Grant Nos. JSZL2022XXXX001), and Shenzhen Municipal Collaborative Innovation Technology Program-International Science and Technology (S&T) Cooperation Project (GJHZ20220913142609017).

AUTHOR DECLARATIONS

Conflict of Interest

The authors have no conflicts to disclose.

Author Contributions

Jingchun Li: Conceptualization (equal); Investigation (equal); Writing – original draft (equal). **Jiaqi Dong:** Supervision (equal). **Zhongbing Shi:** Software (equal). **Wulyu Zhong:** Resources (equal). **Min Xu:** Visualization (equal). **Zhihong Lin:** Methodology (equal); Supervision (equal). **Jun Cheng:** Methodology (equal). **Z. X. Wu:** Conceptualization (equal); Investigation (equal). **Jianqiang Xu:** Formal analysis (equal); Software (equal). **Yu He:** Software (equal). **Zhihui Huang:** Resources (equal). **Anshu Liang:** Data curation (equal). **Tengfei Sun:** Validation (equal).

DATA AVAILABILITY

The data that support the findings of this study are available from the corresponding author upon reasonable request.

REFERENCES

[1]T. E. Evans, Plasma Phys. Controlled Fusion **57**, 123001 (2015).

[2]S. C. McCool, A. J. Wootton, A. Y. Aydemir, R. D. Bengtson, J. A. Boedo, R. V. Bravenec, D. L. Brower, J. S. DeGrassie, T. E. Evans, S. P. Fan, J. C. Forster, M. S. Foster, K. W. Gentle, Y. X. He, R. L. Hickock, G. L. Jackson, S. K. Kim, M. Kotschenreuther, N. C. Luhmann, W. H. Miner, N. Ohyabu, D. M. Patterson, W. A. Peebles, P. E. Phillips, T. L. Rhodes, B. Richards, C. P. Ritz, D. W. Ross, W. L. Rowan, P. M. Schoch, B. A. Smith, J. C. Wiley, X. H. Yu, and S. B. Zheng, Nucl. Fusion **29**, 547 (1989).
[3]S. C. McCool, A. J. Wootton, M. Kotschenreuther, A. Y. Audemir, R. V. Bravenec, J. S. DeGrassie, T. E. Evans, R. L. Hickok, B. Richards, W. L. Rowan, and P. M. Schoch, Nucl. Fusion **30**, 167 (1990).
[4]T. Shoji, H. Tamai, Y. Miura, M. Mori, H. Ogawa, A. W. Leonard, T. Jensen, A. W. Hyatt, A. M. Howald, G. Fuchs, N. Ohyabu, N. Asakura, T. Fujita, M. Shimada, S. Tsuji, H. Maeda, H. Aikawa, K. Hoshino, S. Kasai, T. Kawakami, H. Kawashima, M. Maeno, T. Matsuda, T. Ogawa, T. Seike, N. Suzuki, K. Uehara, T. Yamamoto, T. Yamauchi, T. Hamano, K. Hasegawa, A. Honda, M. Kazawa, Y. Kashiwa, K. Kikuchi, H. Okano, E. Sato, N. Seki, T. Shibata, T. Shiina, S. Suzuki, T. Tani, T. Tokutake, Y. Tomiyama, and T. Yamasato, J. Nucl. Mater. **196–198**, 296 (1992).
[5]R. J. La Haye, Phys. Plasmas **13**, 055501 (2006).
[6]L. Frassinetti, K. E. J. Olofsson, P. R. Brunsell, and J. R. Drake, Nucl. Fusion **50**, 035005 (2010).
[7]G. R. McKee, Z. Yan, C. Holland, R. J. Buttery, T. E. Evans, R. A. Moyer, S. Mordijck, R. Nazikian, T. L. Rhodes, O. Schmitz, and M. R. Wade, Nucl. Fusion **53**, 113011 (2013).
[8]Z. R. Williams, M. J. Pueschel, P. W. Terry, T. Nishizawa, D. M. Kriete, M. D. Nornberg, J. S. Sarff, G. R. McKee, D. M. Orlov, and S. H. Nogami, Nucl. Fusion **60**, 096004 (2020).
[9]M. Vlad and F. Spineanu, Nucl. Fusion **56**, 092003 (2016).
[10]S. C. Liu, Y. Liang, L. T. Li, T. F. Tang, X. H. Wu, N. Yan, T. H. Shi, G. S. Li, K. X. Ye, L. Y. Meng, R. Ding, Y. Sun, M. Jia, Q. Ma, Q. Zang, X. Li, S. X. Wang, M. R. Wang, H. L. Zhao, J. L. Wei, T. Zhang, Y. F. Jin, L. Liao, W. Y. Wei, Y. Li, R. Chen, G. H. Hu, N. Zhao, X. J. Liu, T. F. Ming, X. Han, W. B. Zhang, L. Wang, J. P. Qian, L. Zeng, G. Q. Li, G. S. Xu, X. Z. Gong, X. Gao, and the East Team, Nucl. Fusion **63**, 042003 (2023).
[11]N. Leuthold, W. Suttrop, M. Willensdorfer, G. Birkenmeier, D. Brida, M. Cavedon, M. Dunne, G. D. Conway, R. Fischer, L. Gil, T. Happel, P. Hennequin, A. Kappatou, A. Kirk, P. Manz, R. M. McDermott, J. Vicente, H. Zohm, the Asdex Upgrade Team, and the EUROfusion Mst1 Team, Nucl. Fusion **63**, 046014 (2023).
[12]F. Zhong, T. Zhang, Y. M. Wang, F. Wen, J. Huang, M. F. Wu, G. S. Li, Y. K. Liu, K. N. Geng, H. M. Xiang, K. X. Ye, Z. Zhou, X. Han, L. Y. Meng, L. Wang, Y. W. Sun, and X. Gao, AIP Adv. **11**, 075010 (2021).
[13]M. Willensdorfer, U. Plank, D. Brida, M. Cavedon, G. D. Conway, D. A. Ryan, W. Suttrop, R. Buchholz, M. Dunne, R. Fischer, M. Griener, J. Hobirk, S. Kasilov, A. Kirk, R. M. McDermott, T. Pütterich, G. Tardini, Q. Yu, ASDEX Upgrade Team, and MST1 Team, Phys. Plasmas **29**, 032506 (2022).
[14]L. Schmitz, D. M. Kriete, R. S. Wilcox, T. L. Rhodes, L. Zeng, Z. Yan, G. R. McKee, T. E. Evans, C. Paz-Soldan, P. Gohil, B. Lyons, C. C. Petty, D. Orlov, and A. Marinoni, Nucl. Fusion **59**, 126010 (2019).
[15]H. Zohm, Plasma Phys. Controlled Fusion **38**, 105 (1996).
[16]T. E. Evans, R. A. Moyer, P. R. Thomas, J. G. Watkins, T. H. Osborne, J. A. Boedo, E. J. Doyle, M. E. Fenstermacher, K. H. Finken, R. J. Groebner, M. Groth, J. H. Harris, R. J. La Haye, C. J. Lasnier, S. Masuzaki, N. Ohyabu, D. G. Pretty, T. L. Rhodes, H. Reimerdes, D. L. Rudakov, M. J. Schaffer, G. Wang, and L. Zeng, Phys. Rev. Lett. **92**, 235003 (2004).
[17]T. E. Evans, R. A. Moyer, K. H. Burrell, M. E. Fenstermacher, I. Joseph, A. W. Leonard, T. H. Osborne, G. D. Porter, M. J. Schaffer, P. B. Snyder, P. R. Thomas, J. G. Watkins, and W. P. West, Nat. Phys. **2**, 419 (2006).
[18]E. J. Doyle, W. A. Houlberg, Y. Kamada, V. Mukhovatov, T. H. Osborne, A. Polevoi, G. Bateman, J. W. Connor, J. G. Cordey, T. Fujita, X. Garbet, T. S. Hahm, L. D. Horton, A. E. Hubbard, F. Imbeaux, F. Jenko, J. E. Kinsey, Y. Kishimoto, J. Li, T. C. Luce, Y. Martin, M. Ossipenko, V. Parail, A. Peeters, T. L. Rhodes, J. E. Rice, C. M. Roach, V. Rozhansky, F. Ryter, G. Saibene, R. Sartori, A. C. C. Sips, J. A. Snipes, M. Sugihara, E. J. Synakowski, H. Takenaga, T. Takizuka, K. Thomsen, M. R. Wade, H. R. Wilson, ITPA Transport Physics Topical Group, ITPA Confinement Database, Group Modelling Topical, and ITPA Pedestal and Group Edge Topical, Nucl. Fusion **47**, S18 (2007).
[19]C. Breton, C. De Michelis, M. Mattioli, P. Monier-Garbet, E. Agostini, T. Fall, W. Hess, J. Lasalle, T. E. Evans, A. Grosman, P. Ghendrih, A. L. Pecquet, L. Poutchy, A. Samain, and J. C. Vallet, Nucl. Fusion **31**, 1774 (1991).
[20]Y. Xu, R. R. Weynants, S. Jachmich, M. Van Schoor, M. Vergote, P. Peleman, M. W. Jakubowski, M. Mitri, D. Reiser, B. Unterberg, K. H. Finken, and the Textor Team, Phys. Rev. Lett. **97**, 165003 (2006).
[21]K. H. Finken, S. S. Abdullaev, M. W. Jakubowski, M. F. M. de Bock, S. Bozhenkov, C. Busch, M. von Hellermann, R. Jaspers, Y. Kikuchi, A. Krämer-Flecken, M. Lehnen, D. Schega, O. Schmitz, K. H. Spatschek, B. Unterberg, A. Wingen, R. C. Wolf, O. Zimmermann, and the Textor Team, Phys. Rev. Lett. **98**, 065001 (2007).
[22]P. B. Snyder, N. Aiba, M. Beurskens, R. J. Groebner, L. D. Horton, A. E. Hubbard, J. W. Hughes, G. T. A. Huysmans, Y. Kamada, A. Kirk, C. Konz, A. W. Leonard, J. Lönnroth, C. F. Maggi, R. Maingi, T. H. Osborne, N. Oyama, A. Pankin, S. Saarelma, G. Saibene, J. L. Terry, H. Urano, and H. R. Wilson, Nucl. Fusion **49**, 085035 (2009).
[23]P. H. Diamond, S.-I. Itoh, K. Itoh, and T. S. Hahm, Plasma Phys. Controlled Fusion **47**, R35 (2005).
[24]G. D. Conway, A. I. Smolyakov, and T. Ido, Nucl. Fusion **62**, 013001 (2022).
[25]P. Tamain, A. Kirk, E. Nardon, B. Dudson, B. Hnat, and the Mast Team, Plasma Phys. Controlled Fusion **52**, 075017 (2010).
[26]F. A. Razak and H. J. Jensen, PLoS ONE **9**, e99462 (2014).
[27]M. Xu, X. R. Duan, Y. Liu, X. M. Song, D. Q. Liu, Y. Q. Wang, B. Lu, Q. W. Yang, G. Y. Zheng, X. T. Ding, J. Q. Dong, G. Z. Hao, W. L. Zhong, Z. B. Shi, L. W. Yan, X. L. Zou, Y. Q. Liu, W. Chen, G. L. Xiao, Y. P. Zhang, M. Jiang, Y. M. Hou, J. Cheng, A. S. Liang, X. Y. Bai, J. Y. Cao, Z. Cao, H. T. Chen, C. H. Cui, Z. Y. Cui, L. Delpech, P. H. Diamond, A. Ekedahl, B. B. Feng, G. Giruzzi, S. B. Gong, H. M. He, T. Hoang, M. Huang, Y. Huang, K. Ida, S. Inagaki, M. Isobe, K. Itoh, S. I. Itoh, X. Q. Ji, R. Ke, M. Kobayashi, G. J. Lei, B. Li, G. S. Li, H. J. Li, J. Q. Li, Q. Li, Q. Li, X. D. Li, Y. G. Li, Y. Li, W. C. Mao, D. Mazon, G. R. McKee, S. Morita, L. Nie, J. F. Peng, Y. Peysson, J. Rao, Y. Ren, G. R. Tynan, H. X. Wang, Q. M. Wang, H. L. Wei, F. Xia, X. P. Xiao, W. M. Xuan, Z. Yan, K. Yao, L. M. Yu, Y. Yu, D. L. Yu, B. D. Yuan, B. S. Yuan, J. H. Zhang, Y. Zhou, and Y. Liu, Nucl. Fusion **59**, 112017 (2019).
[28]K. J. Zhao, T. Lan, J. Q. Dong, L. W. Yan, W. Y. Hong, C. X. Yu, A. D. Liu, J. Qian, J. Cheng, D. L. Yu, Q. W. Yang, X. T. Ding, Y. Liu, and C. H. Pan, Phys. Rev. Lett. **96**, 255004 (2006).
[29]J. Cheng, J. Q. Dong, K. Itoh, L. W. Yan, M. Xu, K. J. Zhao, W. Y. Hong, Z. H. Huang, X. Q. Ji, W. L. Zhong, D. L. Yu, S.-I. Itoh, L. Nie, D. F. Kong, T. Lan, A. D. Liu, X. L. Zou, Q. W. Yang, X. T. Ding, X. R. Duan, Y. Liu, and HL-2A Team, Phys. Rev. Lett. **110**, 265002 (2013).
[30]V. I. Demidov, S. V. Ratynskaia, and K. Rypdal, Rev. Sci. Instrum. **73**, 3409 (2002).
[31]K.-S. Chung, Plasma Sources Sci. Technol. **21**, 063001 (2012).
[32]T. Schreiber, Phys. Rev. Lett. **85**, 461 (2000).
[33]B. P. van Milligen, G. Birkenmeier, M. Ramisch, T. Estrada, C. Hidalgo, and A. Alonso, Nucl. Fusion **54**, 023011 (2014).
[34]J. Q. Xu, Y. R. Qu, J. C. Li, Z. Lin, J. Q. Dong, X. D. Peng, M. Jiang, H. P. Qu, Z. H. Huang, N. Wu, W. C. Wang, G. Z. Hao, W. Chen, J. Q. Li, and M. Xu, Nucl. Fusion **62**, 086048 (2022).
[35]M. Wibral, N. Pampu, V. Priesemann, F. Siebenhuhner, H. Seiwert, M. Lindner, J. T. Lizier, and R. Vicente, PLoS ONE **8**, e55809 (2013).
[36]O. Meneghini, S. P. Smith, L. L. Lao, O. Izacard, Q. Ren, J. M. Park, J. Candy, Z. Wang, C. J. Luna, V. A. Izzo, B. A. Grierson, P. B. Snyder, C. Holland, J. Penna, G. Lu, P. Raum, A. McCubbin, D. M. Orlov, E. A. Belli, N. M. Ferraro, R. Prater, T. H. Osborne, A. D. Turnbull, and G. M. Staebler, Nucl. Fusion **55**, 083008 (2015).
[37]C. Hidalgo, Plasma Phys. Controlled Fusion **37**, A53 (1995).
[38]M. Leconte, P. H. Diamond, and Y. Xu, Nucl. Fusion **54**, 013004 (2014).
[39]J. M. Beall, Y. C. Kim, and E. J. Powers, J. Appl. Phys. **53**, 3933 (1982).
[40]N. Mahdizadeh, F. Greiner, M. Ramisch, U. Stroth, W. Guttenfelder, C. Lechte, and K. Rahbarnia, Plasma Phys. Controlled Fusion **47**, 569 (2005).
[41]P. H. Diamond and Y. -B. Kim, Phys. Fluids B **3**, 1626 (1991).
[42]J. E. Rice, Plasma Phys. Controlled Fusion **58**, 083001 (2016).
[43]M. Leconte and R. Singh, Phys. Plasmas **25**, 082311 (2018).
[44]W. L. Zhong, Z. B. Shi, X. L. Huang, Z. T. Liu, W. Chen, M. Jiang, J. Li, Z. Y. Cui, X. M. Song, L. Y. Chen, X. L. Zou, X. T. Ding, Y. Liu, L. W. Yan, Q. W. Yang, and X. R. Duan, Rev. Sci. Instrum. **85**, 013507 (2014).